SPE 30714

Modeling Gas Condensate Well Deliverability

Ø. Fevang, SPE, and C.H. Whitson, SPE, U. Trondheim, NTH

Abstract

This paper gives an accurate method for modeling the deliverability of gas condensate wells. Well deliverability is calculated using a modified form of the Evinger-Muskat[1] pseudopressure (originally proposed for solution gas drive oil wells). The producing GOR is needed to calculate pseudopressure, together with PVT properties (black-oil or compositional), and gas-oil relative permeabilities. The proposed method is successfully tested for radial, vertically fractured, and horizontal wells.

Using the proposed deliverability model, we show that fine-grid single-well simulations can be reproduced almost exactly with a simple rate equation using pseudopressure. The key is knowing the producing GOR accurately. The effect of near-wellbore damage, vertical fracture, or flow improvement due to horizontal well trajectory is readily incorporated into the rate equation as a constant skin term.

The effect of gas-oil relative permeability is studied. We show that well deliverability impairment due to near-wellbore condensate "blockage" is only dependent on the relative permeabilities within the range defined by $1<k_{rg}/k_{ro}<50$. Usually this represents gas and oil relative permeabilities ranging from 0.05 to 0.3. Gas relative permeabilities at low oil saturations ($k_{rg}>0.3$) only affect deliverability for richer gas condensates (with maximum liquid dropout of 10% or greater).

A key observation and conclusion from this study is that critical oil saturation has *no* direct effect on well deliverability. We also show that IFT-dependence of relative permeability has little or no effect on gas condensate well performance (e.g. length of plateau production).

The most important application of this study is to provide a simple method for calculating bottomhole flowing pressure (BHFP) in coarse-grid models. We show that the proposed pseudopressure method is readily calculated for each well grid cell based only on grid cell pressure and producing GOR. Local grid refinement near wells is not necessary, and relatively large well grid cells can be used while still providing an accurate description of well deliverability.

Based on our analysis of the three basic flow regions of a gas condensate well, and the large effect of near-wellbore condensate blockage on well deliverability, we propose an experimental procedure for measuring relative permeabilities (specifically for modeling well deliverability).

Introduction

Calculation of gas condensate well deliverability has been a long-standing problem, without a simple solution. When BHFP drops below the dewpoint, a region of high condensate saturation buildups up near the wellbore, resulting in reduced gas permeability and lower gas deliverability. The effect of a condensate blockage region depends on relative permeability and PVT properties, and how the well is being produced.

Obviously, reduced gas deliverability due to condensate blockage is *only* important when the BHFP reaches a minimum (dictated by surface constraints) and the well is forced to go on decline.

Muskat[2] addresses the condensate blockage problem in his discussions of gas cycling, where he introduces a simple method for estimating the radius of condensate blockage as a function of time, gas rate, and reservoir rock and fluid properties. Fetkovich[3] uses Muskat's results to derive a rate- and time-dependent blockage skin for use in the standard gas rate equation.

Kniazeff and Naville[4] and Eilerts et al.[5,6] were the first to numerically model radial gas condensate well deliverability. These studies show radial saturation and pressure profiles as a function of time and other operational variables, confirming that condensate blockage reduces well deliverability. Kniazeff and Naville also study the effect of non-Darcy flow (in the gas phase) on well deliverability.

Gondouin et al.[7] make a significant contribution towards the fundamental understanding of gas condensate well deliverability. Through radial black-oil simulations, they extend the work by Kniazeff and Naville, showing the importance of

condensate blockage and non-Darcy flow effects on backpressure performance. They also give experimental procedures and measurements that quantify the effects of relative permeability and *multiphase* non-Darcy flow.

O'Dell and Miller[8] present the first gas rate equation using a pseudopressure function to describe the effect of condensate blockage. The equation is valid when (1) produced wellstream is the original reservoir gas, and (2) the blockage radius is relatively small (i.e. the reservoir pressure is significantly above the dewpoint). From their results, it is clear that well deliverability can be significantly reduced even for small regions of condensate blockage.

Fussell[9] presents EOS compositional simulations of radial gas condensate wells producing by pressure depletion below the dewpoint. He shows that the O'Dell-Miller equation (with a small correction to account for gas dissolved in the flowing oil phase) dramatically overpredicts the deliverability loss due to condensate blockage, compared with simulation results.

Jones and Raghavan[10,11] treat, for the most part, transient pressure behavior (drawdown and buildup) of radial wells. They use EOS compositional simulation with simple three-component (C_1-C_4-C_{10}) gas condensate mixtures. The key observation made concerning long-term ("boundary-dominated") well deliverability, is that the pseudopressure function presented by Fussell is accurate at all times during depletion. However, the integral must be evaluated using pressures and saturations known as a function of radius at a given time in depletion ("reservoir integral pseudopressure"). However, as they point out themselves, this isn't very helpful because they have to do compositional simulation to know the pressures and saturations at a given time in depletion. We show in this paper how to easily get the pressures and saturations from the instantaneous producing GOR (i.e. the producing wellstream composition).

Gas Condensate Rate Equation

The general volumetric rate equation for a gas condensate well of any geometry (e.g. radial, vertically fractured, or horizontal) is, for a compositional formulation,

$$q_g = C \left(\frac{RT_{sc}}{p_{sc}} \right) \beta_s \int_{p_{wf}}^{p_R} \left(\frac{\rho_o k_{ro}}{M_o u_o} + \frac{\rho_g k_{rg}}{M_g \mu_g} \right) dp \quad \cdots\cdots\cdots \quad (1)$$

or in terms of black-oil PVT,

$$q_g = C \int_{p_{wf}}^{p_R} \left(\frac{k_{ro}}{B_o \mu_o} R_s + \frac{k_{rg}}{B_{gd} \mu_g} \right) dp \quad \cdots\cdots\cdots\cdots \quad (2)$$

where

$$C = \frac{2\pi a_1 k h}{\ln(r_e/r_w) - 0.75 + s} \quad \cdots\cdots\cdots\cdots\cdots \quad (3)$$

$a_1 = 1/(2\pi \cdot 141.2)$ for field units, and $a_1 = 1$ for pure SI units. The constant C includes basic reservoir properties such as permeability k, thickness h, drainage radius r_e, wellbore radius r_w, and other constants. Relative permeabilities k_{rg} and k_{ro} are defined relative to *absolute permeability*, and *not* relative to permeability at irreducible water saturation (this distinction is

particularly important when correlating relative permeability data).

Skin s is a composite factor that includes non-ideal flow effects such as damage, stimulation, drainage geometry, and partial penetration. The traditional approach for estimating[12] or measuring[13] composite skin for a well producing single-phase fluid can be used to determine skin.

The condensate blockage effect is treated separately by the pseudopressure integral. We show that the pseudopressure integral, if evaluated properly, is for practical purposes independent of well geometry. This greatly simplifies the treatment of gas condensate well deliverability.

Flow Regions. An accurate yet simple model of a gas condensate well undergoing depletion consists of three regions:

Region 1: An inner near-wellbore region where both gas and oil flow simultaneously (at different velocities).

Region 2: A region of condensate buildup where only gas is flowing.

Region 3: A region containing single phase (original) reservoir gas.

For a given producing condition, one, two, or all three regions may exist. These three regions define pseudosteady-state flow conditions, meaning that they represent steady-state conditions at a given time but that the steady-state conditions change gradually during depletion.

Region 1. The *flowing* composition (GOR) within Region 1 is constant throughout. That means that the single-phase gas entering Region 1 has the same composition as the produced wellstream mixture. Conversely, if we know the producing wellstream, then we know the flowing composition within Region 1. Furthermore, the dewpoint of the producing wellstream mixture equals the reservoir pressure at the outer edge of Region 1.

Region 1 is the main source of deliverability loss in a gas condensate well. Gas relative permeability is reduced due to condensate buildup. The size of Region 1 increases with time. For steady-state conditions, the condensate saturation in Region 1 is determined (as a function of radius) *specifically* to ensure that all liquid that condenses from the single-phase gas entering Region 1 has sufficient mobility to flow through and out of Region 1 without any net accumulation.

Region 2. If it exists (as it usually does), Region 2 defines a region of net accumulation of condensate. Effectively, only gas is flowing in this region because oil mobility is zero (or very small). Condensate saturations in Region 2 are closely approximated by the liquid dropout curve from a constant volume depletion (CVD) experiment[14], corrected for water saturation.

The size of Region 2 is largest at early times just after the reservoir pressure drops below the dewpoint. It decreases in size with time because Region 1 is expanding. The size and importance of Region 2 is greater for lean gas condensates.

The main consequence of Region 2 is that producing wellstream composition (GOR) is leaner than calculated by a simple volumetric material balance (e.g. CVD measurements). Incorrect use of material balance GORs in the calculation of

the pseudopressure significantly overestimates deliverability loss in Region 1, especially at early times in depletion just after reservoir pressure drops below the dewpoint.

Region 3. Region 3 will always (and only) exist in a gas condensate reservoir that is currently undersaturated. The standard treatment[15] of single phase gas flow is used to quantify the contribution of Region 3 to well deliverability. Composition is constant in Region 3, equal to the original reservoir gas.

Coexistence of Flow Regions. If FBHP is less than the dewpoint, Region 1 will always exist (after a short transient required to build up the steady-state saturations in Region 1). Region 1 will not exist if FBHP is greater than the dewpoint.

Region 2 will always exist together with Region 1 after reservoir pressure drops below the dewpoint. In this case, Region 3 will not exist.

All three regions exist for reservoirs that are slightly undersaturated and FBHP is less than the dewpoint. Region 2 may "disappear" or have negligible effect for highly undersaturated reservoirs.

It is not possible for Regions 2 and 3 to exist in the absence of Region 1 (after steady-state conditions are reached).

For a very rich (near-critical) gas condensate, Region 1 may exist *throughout* the drainage area (in the absence of Regions 2 and 3), after reservoir pressure drops below the dewpoint.

Calculating Pseudopressure. Based on our observations of the three flow regions for many gas condensate systems, we have developed a simple method to accurately calculate the pseudopressure integral in Eqs. (1) and (2). The approach is an extension of the pseudopressure method proposed by Evinger and Muskat for solution gas drive oil wells.

First we break the pseudopressure integral into three parts, corresponding to the three flow regions discussed above.

$$\underline{\text{Total}} \qquad \Delta p_p = \int_{p_{wf}}^{p_R} \left(\frac{k_{rg}}{B_{gd}\mu_g} + \frac{k_{ro}}{B_o\mu_o} R_s\right) dp =$$

$$\underline{\text{Region 1}} \qquad \int_{p_{wf}}^{p*} \left(\frac{k_{rg}}{B_{gd}\mu_g} + \frac{k_{ro}}{B_o\mu_o} R_s\right) dp \quad +$$

$$\cdots \text{(4)}$$

$$\underline{\text{Region 2}} \qquad \int_{p*}^{p_d} \frac{k_{rg}}{B_{gd}\mu_g} dp \quad +$$

$$\underline{\text{Region 3}} \qquad k_{rg}(S_{wi}) \int_{p_d}^{p_R} \frac{1}{B_{gd}\mu_g} dp$$

Given the producing GOR R_p, we know immediately p* because it equals the dewpoint of the producing wellstream. Using black-oil PVT, with r_s defined as the solution oil-gas ratio, we locate the pressure in the PVT table where $r_s = 1/R_p$ and define this pressure as p*. In a compositional treatment the dewpoint of the producing wellstream composition is defined

as p*. If $p* > p_R$, then integration of the Region 1 integral should only be from p_{wf} to p_R; in this case, Regions 2 and 3 don't exist.

Region 1. The Region 1 pseudopressure integral is solved using the modified Evinger-Muskat approach. At pressures $p < p*$ the PVT properties R_s, B_o, r_s, B_{gd}, μ_o, and μ_g are found directly. Next, the equation defining producing GOR[16]

$$R_p = R_s + \left(\frac{k_{rg}}{k_{ro}}\right)\left(\frac{\mu_o B_o}{\mu_g B_{gd}}\right)(1 - r_s R_p) \cdots \cdots \text{(5)}$$

is used to calculate k_{rg}/k_{ro} as a function of pressure,

$$\frac{k_{rg}}{k_{ro}}(p) = \left(\frac{R_p - R_s}{1 - r_s R_p}\right)\frac{\mu_g B_{gd}}{\mu_o B_o} \cdots \cdots \text{(6)}$$

where PVT properties are known as a function of pressure. It is readily shown that Eq. (6) can be expressed in terms of the oil relative volume of the flowing gas during a constant composition expansion, $V_{roCCE} = V_o/(V_g + V_o)$,

$$\frac{k_{rg}}{k_{ro}}(p) = \left(\frac{1}{V_{roCCE}} - 1\right)\frac{\mu_g}{\mu_o} \cdots \cdots \text{(7)}$$

From Eqs. (6) and (7), V_{roCCE} can be expressed in terms of black-oil PVT properties, for any producing GOR R_p,

$$V_{roCCE}(p) = \left[1 + \left(\frac{R_p - R_s}{1 - r_s R_p}\right)\frac{B_{gd}}{B_o}\right]^{-1} \cdots \cdots \text{(8)}$$

As shown by Evinger and Muskat, relative permeabilities k_{rg} and k_{ro} can be expressed directly as a function of the ratio k_{rg}/k_{ro} (when both phases are mobile). This means that we can evaluate k_{rg} and k_{ro} directly as a function of pressure in the Region 1 pseudopressure integral, $k_{rg}(p) = f[k_{rg}/k_{ro}(p)]$ and $k_{ro}(p) = f[k_{rg}/k_{ro}(p)]$, using Eq. (6).

Region 2. When Region 2 exists ($p* < p_R$), the Region 2 integral is evaluated using $k_{rg}(S_o)$, where S_o is estimated as a function of pressure from CVD relative oil volumes $V_{roCVD}(p) = V_o(p)/V_d$, yielding $S_o(p) = [V_{roCVD}(p)](1 - S_w)$. If V_{roCVD} values are not known for the black-oil PVT data set, they can be calculated using the following equations:

$$(V_{roCVD})_k = \frac{N_{k-1} - G_{k-1}(r_s)_k}{1 - (r_s R_s)_k}(B_o)_k$$

$$N_{k-1} = \left(\frac{V_{roCVD}}{B_o} + \frac{1 - V_{roCVD}}{B_{gd}} r_s\right)_{k-1} \cdots \cdots \text{(9)}$$

$$G_{k-1} = \left(\frac{V_{roCVD}}{B_o} R_s + \frac{1 - V_{roCVD}}{B_{gd}}\right)_{k-1}$$

where k represents the current pressure, k-1 represents the previous pressure, and $(V_{roCVD})_0 = 0$.

Region 3. Only PVT properties are found in the Region 3 integral, where the traditional single-phase gas pseudopressure function can be used.

Verification of Proposed Pseudopressure Approach
To illustrate the proposed method for determining gas rate from Eq. (2), with pseudopressure calculated using the

proposed method outlined above, we have simulated several examples. We use two gas condensate fluids with radial, vertically fractured, and horizontal well geometries.

The two fluids are: *Rich Gas A*, an undersaturated gas condensate with 175 STB/MMscf and a maximum CVD liquid dropout of 23%; and *Lean Gas B*, a slightly undersaturated gas condensate with 45 STB/MMscf and a maximum CVD liquid dropout of 2%. PVT properties[14] for the two fluids are shown in **Figs. 1-4**. The reservoir properties and numerical grids are given in **Tables 1 and 2**. The gas/oil relative permeability data are calculated using a Corey equation.[17] Set A curves are shown in **Fig. 5**, and unless otherwise state, these curves are used in all calculations.

Compositional vs. Black-Oil PVT Formulation. Coats[18] presents radial well simulations that show a modified black-oil PVT formulation gives the same results as a fully compositional EOS PVT formulation. Results are given for a rich gas condensate producing on decline for 8 years. The EOS characterization uses seven components with one C_{7+} fraction.

Results from this example should probably be used with caution. A serious limitation is that only one C_{7+} fraction is used. With a more detailed C_{7+} split, oil viscosity differences between black-oil and compositional formulations often yield noticeable differences in well deliverability.

The problem is illustrated in **Fig. 6** where oil viscosity is plotted versus pressure. The solid line represents black-oil data, and the symbols represent results taken from compositional simulation of Rich Gas A. The figure shows that oil viscosities can change significantly during depletion.

Because the oil mobility required to flow condensed oil in Region 1 is basically fixed, a lower oil viscosity in the compositional simulations (particularly near the wellbore) results in a lower oil relative permeability and lower oil saturation than in the black-oil simulations; lower oil saturation results in higher gas relative permeability and better well deliverability for the compositional simulations (**Fig. 7**).

This problem can be improved using a modified $\mu_o(p)$ relationship in the black-oil simulator. The dashed line in **Fig. 6** passes through the "important" compositional results (data at pressures lower than the point where μ_o reaches a minimum). This same trend can be determined using a PVT simulator. When the modified $\mu_o(p)$ relation is used in black-oil reservoir simulation, well performance is closer to compositional results (dashed line in Fig. 7).

Pseudopressure Calculations. Gas rate is calculated with the *"Proposed Method"* for determining pseudopressure in Eq. (2), using the same black-oil PVT data as used in the simulation; the producing GOR, BHFP, and average reservoir pressure, as a function of time, are taken from the simulator.

Gas rate is also calculated using the same pseudopressure function, but with producing GOR set equal to $1/r_s$, evaluated at p_R; once again, the BHFP and average reservoir pressure, as a function of time, are taken from the simulator. This approach is equivalent to using a material balance based on a simple CVD depletion process (*"CVD MB Method"*), which also implies that Region 2 doesn't exist.

Radial Well - Lean Gas B. The Lean Gas B production forecast for a radial well is shown in **Fig. 8**, with simulated black-oil results shown as symbols. The solid line represents gas rate calculated with the Proposed Method to evaluate the pseudopressure (using R_p, p_R, and p_{wf} from the simulator). The PI constant C in Eq. (2) is calculated from Eq. (3) with s=0. Results are excellent.

The dashed line represents gas rate calculated with the same pseudopressure function [Eq. (2)], also using p_R and p_{wf} from the simulator, but using $R_p=1/r_s$ (with r_s evaluated at p_R). Results are poor, with well deliverability highly underestimated. The dot-dashed line uses the same CVD MB Method but with $p_{wf} = p_{wfmin} = 1500$ psia for all times.

The difference in rates calculated with the Proposed Method and the CVD MB Method is largest at early times. The reason is that Region 2 is largest at early times, decreasing in size with time.

Radial Well - Rich Gas A. The same radial well simulation is run with Rich Gas A. Results are given in **Fig. 9**, where the Proposed Method for evaluating pseudopressure reproduces the simulated results almost exactly. The simplified CVD MB Method gives good results for only a short time while the reservoir is still sufficiently undersaturated that producing GOR equals the initial solution GOR ($1/r_{si}$). As soon as R_p deviates from $1/r_s(p_R)$, the CVD MB Method starts to overestimate deliverability loss.

Vertically Fractured Well - Rich Gas A. A vertical fracture was simulated using the 2D cartesian grid given in Table 3 (420 grid cells). Results are plotted as symbols in **Fig. 10**.

Before making calculations with Eq. (2), the productivity index C had to be determined. We simulated the well with single-phase gas at high pressure (10,000 psia) to back-calculate C from pseudosteady state pressure performance. Using the Proposed Method for calculating pseudopressure, we obtained the rates given by a solid line in Fig. 10. The results are very accurate, with only slight deviation at late times.

Calculations based on the CVD MB Method with $R_p=1/r_s(p_R)$ underpredicts well deliverability at all times. Again, the largest deviations occur when Region 2 is largest (1-3 years).

Horizontal Well - Rich Gas A. A horizontal well was simulated using the 3D cartesian grid given in Table 3 (2223 grid cells). Results are given as symbols in **Fig. 11**.

Before making calculations with Eq. (2), the productivity index C had to be determined. We simulated the well with single-phase gas at high pressure (10,000 psia) to back-calculate C from pseudosteady state pressure performance. Using the Proposed Method for calculating pseudopressure, results are very accurate throughout the 20 year production period (solid line in Fig. 11).

Calculations based on the CVD MB Method with $R_p=1/r_s(p_R)$ underpredicts well deliverability at all times. The largest deviations occur when Region 2 has most effect (1-3 years).

Note that the well deliverability of a well with a 50-foot vertical fracture half-length is the same as the deliverability of a 1000-foot horizontal well! This result is for a typical k_v/k_h ratio of 0.1. Using $k_v/k_h=1$, the plateau period increases from 3.0 to 9.5 years. This extreme sensitivity to k_v/k_h does not exist for vertically fractured wells, and if horizontal wells are being considered in the development of a gas condensate reservoir, the k_v/k_h ratio should be determine with certainty to avoid overly optimistic production forecasts.

Application to Coarse-Grid Field Models

The main conclusion from the comparisons above is that the Proposed Method for calculating the gas rate pseudopressure function for a gas condensate well is accurate as long as the producing GOR is known accurately, independent of well geometry and production mode. Given this observation, we decided to evaluate the accuracy of producing GORs predicted by coarse-grid simulations.

Results show that coarse-grid GORs are generally very accurate. Consequently, the Proposed Method for calculating pseudopressure function of a gas condensate well can be used to accurately convert coarse grid cell pressures to BHFPs (individually for each well grid cell).

Conversion from grid cell pressure to BHFP for a gas well is usually made with the radial flow equation and a well index J, where $p_{wf} = p_{grid} - q_g/J$, with J given by

$$J = C \frac{k_{rg}}{\mu_g B_{gd}} \dots\dots\dots\dots\dots\dots\dots\dots\dots\dots\dots (10)$$

where k_{rg}, μ_g, and B_{gd} are evaluated at conditions in the well grid cell. Our proposal is simply to replace the $k_{rg}/\mu_g B_{gd}$ term with the pseudopressure integral defined in Eqs. (2) and (4), evaluating the integral from p_{wf} to p_{grid}.

Although Peaceman's equation(s)[19] can be used to calculate J (or C), we consistently found that it was better to determine the well index using results from single-phase simulations with a fine grid.

In a simulator, all PVT and relative permeability properties are available in each grid cell. For the sake of efficiency, the pseudopressure function Δp_p can be calculated during initialization for several producing GORs, and then stored as a three-dimensional table $\Delta p_p(p_{wf}, p_{grid}, R_p)$. Conceivably a different Δp_p function needs to be generated for all PVT/relative permeability regions. In the most general case, Δp_p can be stored as a four-dimensional table to handle changing water saturations, $\Delta p_p(p_{wf}, p_{grid}, R_p, S_w)$.

We wanted to test the proposed application using a commercial reservoir simulator. Intera's ECL100 was used, but because we did not have access to source code, it was necessary to incorporate the pseudopressure table as a "pseudo" tubing table. First we introduced an "infinite" well index J so that the model-calculated BHFP equals the well-grid-cell pressure. The pseudo-tubing table then converts this (well-grid-cell) pressure to actual BHFP [using Eq. (2)], based on gas rate and producing GOR.

The pseudo-tubing table approach can be used as a general solution to problems where the well produces from layers that are in vertical communication (i.e. experiencing reservoir crossflow). However, the approach is not recommended for wells producing from layered no-crossflow systems. The best general solution is to have the well pseudopressure tables generated at initialization, so that any grid cell that becomes a well grid will automatically have the multiphase pseudopressure method available.

Coarse Radial Grid. The size of the first grid cell in a radial simulation can be important in modeling well deliverability of gas condensates. This is shown in **Fig. 12**, where Lean Gas B is used with a first-grid cell radius of 100 ft (versus 0.7 ft in the fine-grid simulation); the remaining grids are spaced logarithmically. The plateau period is more than doubled from 2.5 for the fine-grid simulation to 6.25 years for the coarse grid simulation. Even for an 18 ft inner radius, the plateau period is overpredicted by more than one year.

Using the multiphase pseudopressure method (based on a pseudo-tubing curve), the correct plateau period of 2.5 years is predicted and the rate-time performance overlays the fine-grid simulation results. Using the same coarse radial grid ($r_1=100$ ft) and Rich Gas A, the proposed pseudoporessure method again predicts the rate-time performance accurately (**Fig. 13**).

Coarse Cartesian Grid. Using a coarse cartesian grid with a 200x200 ft well grid cell, the proposed method was compared with the fine-grid radial simulation for Lean Gas B. Results are shown in **Fig. 14**, where the rate-time performance is accurately calculated using the coarse grid pseudopressure method. Note that the standard well treatment [Eq. (10)] results in a plateau of 6 years compared with the correct plateau of 2.5 years.

Using a coarse cartesian grid with a 500x500 ft well grid cell, the proposed method was compared with 2D fine-grid simulation results of a vertically fractured well using Rich Gas A. **Fig. 15** shows that the rate-time performance is accurately calculated using the coarse grid pseudopressure method. The standard well treatment results in a plateau of 6 years compared with the correct plateau of 3 years.

Using a coarse cartesian grid with 333x333x25 ft well grid cells, the proposed method was compared with fine-grid 3D horizontal well simulation results for Rich Gas A. Results are shown in **Fig. 16**, where the rate-time performance is accurately calculated using the coarse grid pseudopressure method. The standard well treatment results in a plateau of almost 6 years compared with the correct plateau of 3 years.

Discussion of Coarse Grid Pseudopressure Method. We have shown that local grid refinement in gas condensate wells is not necessary. The only limitation of the pseudopressure approach is that producing GOR from the coarse grid model is reasonably accurate (compared with fine grid simulation).

Effectively, Region 2 is eliminated *in the well grid cell* using this approach. Surrounding grid cells, however, automatically treat the Region 2 pressures losses. The more important Region 1 behavior is treated accurately in the well grid cell. However, if the size of the well grid cell becomes too large, Region 1 pressure losses will be overestimated and calculated well deliverability underestimated. In the limit of one grid cell describing the entire drainage area, this method becomes equivalent to the CVD MB Method, which always underestimates well deliverability.

Deciding an appropriate well grid size will depend on (1) the leanness of the gas condensate, (2) the minimum well plateau length, and (3) the degree of undersaturation. Smaller well grids are needed for lean gas condensates, short plateau periods, and initially saturated fluids. In other words, a saturated lean gas condensate that goes on decline immediately will require the smallest well grid size.

A few sensitivity cases can be run to determine the required well grid size for a given gas condensate reservoir. These cases should evaluate wells producing at the maximum expected rate (dictated by equipment constraints such as tubing diameter and erosional velocity). A case with initial pressure equal to the dewpoint should be used, even for highly undersaturated reservoirs, to evaluate a "late" well being drilled after depletion to the dewpoint.

Relative Permeability Effects

Primary Functional Relationship $k_{rg} = f(k_{rg}/k_{ro})$. The deliverability loss due to condensate blockage is dictated by the Region 1 contribution to the pseudopressure integral. This contribution is solved by finding the relationship between k_{rg} and the ratio k_{rg}/k_{ro}. **Fig. 17** shows a plot of k_{rg} vs. k_{rg}/k_{ro} based on the Corey equation for different pore size distribution parameters λ.

The relevant range of k_{rg}/k_{ro} found in Region 1 can be calculated directly from PVT properties and Eq. (6) as a function of pressure, from the dewpoint pressure *of the flowing mixture* (wellstream) to any lower pressure.

Calculation of $k_{rg}/k_{ro}(p)$ from Eq. (7) can be done readily with a PVT simulator. Results for both Gases A and B are shown in Figs. **18-19**, together with plots of $V_{roCCE}(p)$. The $k_{rg}/k_{ro}(p)$ plot defines the lower range of relative permeabilities of interest. The upper limit on relevant k_{rg}/k_{ro} ranges from 10 for rich condensates to about 50 for lean condensates. Accordingly, the range of relative permeabilities to be measured in the laboratory are defined from the $k_{rg}/k_{ro}(p)$ plot (Appendix A).

Returning to Fig. 17 (k_{rg} vs. k_{rg}/k_{ro}), we show for different gas condensate fluids the practical range of k_{rg}/k_{ro} existing in Region 1. An upper limit of 50 will practically apply for all gas condensates because (1) the k_{rg} value is relatively high at $k_{rg}/k_{ro}>50$, (2) only a small pressure interval just below the wellstream dewpoint experiences this range of k_{rg}/k_{ro} (at the outer edge of Region 1), and (3) if k_{rg} vs. k_{rg}/k_{ro} is well defined experimentally at $k_{rg}/k_{ro}<50$, then the extrapolation to higher k_{rg}/k_{ro} values is trivial.

To illustrate the importance of the k_{rg} vs. k_{rg}/k_{ro} relationship for well deliverability, we first simulated a radial well for Rich Gas A using relative permeability Set B (shown as solid lines in **Figs. 20-21**).

For this relatively rich fluid we assume that the relevant range of relative permeabilities in Region 1 is limited by $k_{rg}/k_{ro}<10$. We then made a second radial simulation using a second set of relative permeabilities (Set B') with an identical $k_{rg}=f(k_{rg}/k_{ro})$ relationship for all saturations (**Fig. 22**), but with completely different $k_{rg}(S_g)$ and $k_{ro}(S_g)$ curves in the range $k_{rg}/k_{ro}<10$ (Figs. 20 and 21).

Simulations of rate-time performance using relative permeability Sets B and B' are shown in **Fig. 23**. The well performs identically, for practical purposes, with both sets of relative permeabilities. These results are *not* a special case, but they are generally true for all gas condensate reservoirs. k_{rg} vs. k_{rg}/k_{ro} *is* the fundamental relative permeability relationship dictating Region 1 behavior and well deliverability, not k_{rg} and k_{ro} as a function of saturation.

Critical Oil Saturation. It has been suggested that S_{oc} is an important parameter in defining relative permeabilities of gas condensates. The only reason this claim can be made is that S_{oc} has been used in parametric equations where effective oil saturation S_o^* is normalized with S_{oc}, e.g.

$$k_{ro} = (S_o*)^2 \left(\frac{S_o}{1-S_{wi}}\right)^{(2+\lambda)/\lambda}$$

$$S_o* = \frac{S_o - S_{oc}}{1-S_{wi}-S_{oc}} \qquad \ldots \ldots \ldots \ldots \ldots \ldots (11)$$

When this is done, a change in S_{oc} affects k_{ro}, and consequently k_{rg}/k_{ro}, at *all* saturations. The result is a totally different $k_{rg} = f(k_{rg}/k_{ro})$ relationship, even though $k_{rg}(S_g)$ is unchanged.

In the absence of relative permeability data, or if available data are questionable, it is a bad idea to make "sensitivity" studies of relative permeability using S_{oc} as a parameter in a general correlation. Instead, the $k_{rg}=f(k_{rg}/k_{ro})$ relationship (in the range $1<k_{rg}/k_{ro}<50$) should be varied systematically, for example using pore size distribution λ in the Corey equation. If S_{oc} *is* used as a parameter in sensitivity studies, the effect it has on well deliverability should be recognized as the effect S_{oc} has on the $k_{rg} = f(k_{rg}/k_{ro})$ relationship, and not on k_{ro} or k_{rg} values near S_{oc}.

Because Region 1 flow behavior dictates well deliverability loss due to condensate blockage, and because oil saturation, oil relative permeability, and oil mobility are all at a maximum in Region 1, the low-oil-saturation relative permeabilities (near S_{oc}) are irrelevant to condensate blockage.

For richer condensates, Region 2 may have oil saturations somewhat greater than S_{oc}. Even so, the oil relative permeability in this saturation region is irrelevant because oil mobility is practically zero. Furthermore, gas relative permeability at low oil saturations is not affected directly by S_{oc}.

To illustrate the insignificance of S_{oc}, Rich Gas A was simulated with radial and vertically fractured well geometries using Set A relative permeabilities (S_{oc}=10%). Rate-time performance for the two wells are shown as solid lines in **Fig. 24**.

For this fluid, the important region of k_{rg}/k_{ro} is less than 10 for most of depletion. Based on this observation, we modified the k_{ro} curve at saturations where k_{rg}/k_{ro} is greater than 10 (low S_o values). Extrapolations of k_{ro} using S_{oc}=0% and S_{oc}=20% are shown in **Fig. 25**. As seen in Fig. 24, the simulated rate-time performance is practically identical for S_{oc}=0% and 20%, compared with the base case using S_{oc}=10%.

We also ran simulations at lower BHFP (250 psia) to see if low oil saturations in Region 1 due to vaporization would result in significant differences in well deliverability for the three oil relative permeability curves with different S_{oc} values. As seen in **Fig. 26**, the effect is very small.

Gas-Oil Interfacial Tension. Probably the most misleading and deceptive concept put forth by earlier publications on gas condensates is the importance of gas-oil IFT on relative permeabilities. Many workers have discussed the potential effect, functional dependence, and methods for measuring the IFT effect on relative permeabilities. But no one has yet shown that reservoir performance is significantly altered by "straightened-line" relative permeabilities due to low IFTs.

The two reservoir mechanisms that are affected by relative permeabilities in gas condensate reservoirs are (1) well deliverability and (2) gravity segregation of condensate that theoretically can occur in high-permeability or fractured reservoirs.

The physics of IFT effect on relative permeabilities is not well understood. Measurements quantifying the effect in a systematic way are lacking, and the data available are not reliable enough to build a theoretical (or empirical) model for predicting the effect. The existing conceptual model states that IFTs must be lower than a "threshold" IFT $\sigma*$ before relative permeabilities are affected. Furthermore, as IFT approaches zero the relative permeabilities approach straight lines with zero residual saturations. The model is given by

$$k_r = F\,k_{r,Immiscible} + (1-F)\,k_{r,Miscible}$$

$$S_r = F\,S_{r,Immiscible}$$

$$k_{r,Miscible} = (S-S_r)/(1-S_{wi}-S_r) \qquad \cdots\cdots\cdots (12)$$

$$F = (\frac{\sigma}{\sigma*})^n \;,\; \sigma<\sigma* \;\;;\;\; F = 1 \;,\; \sigma\geq\sigma*$$

Recent measurements indicate that $\sigma*$ ranges from 0.1 to 0.3 mN/m. Exponent n=0.1 is recommended, though this is based more on physical intuition than experimental evidence.

In this paper we deal mostly with the potential effect of IFT on well deliverability. We also have studied gravity segregation, with the following observations: (1) segregation is negligible unless permeability is high (> 1000 md) and near-straight-line relative permeability curves exist, (2) the low-IFT period just below the dewpoint (with near-straight-line curves)

is short-lived, (3) IFTs exceeding the "threshold" IFT (ranging from 0.1 to 0.3 mN/m) exist during the major part of depletion even for near-critical systems (see **Fig. 27**); IFT effect on relative permeability is nonexistent for IFTs exceeding the threshold IFT.

Consequently, we do not see how it is possible to develop significant condensate accumulations by gravity segregation. Our simulations indicate that such accumulations do not develop unless straight-line curves are used throughout depletion, and physically this can only be expected in a single-porosity fractured reservoir (where relative permeabilities are basically independent of IFT!). Finally, even if some segregation does occur, it is difficult to conceptualize a reservoir development strategy that would be economically competitive with gas cycling. Blue sky!

Concerning the effect of IFT on well deliverability, we have made the following observations (which are supported by simulations presented below): (1) Gas condensate reservoirs will generally never experience IFTs lower than threshold IFTs of 0.1 to 0.3 mN/m in near-wellbore Region 1, *when BHFP reaches a minimum and the well goes on decline.* (2) Low IFT in Region 2 and the resulting improvement in gas relative permeability has only a minor effect (if any) on deliverability.

Simulation of a "worst" case using Rich Gas A is given for radial and vertically fractured wells. The IFT model given by Eq. (12) uses Set A "Immiscible" relative permeability curves, $\sigma*$=0.3 mN/m, and n=0.1. Simulated rate-time performance is shown in **Figs. 28**-**29**, indicating relatively little effect of IFT-corrected relative permeabilities on well deliverability. Absolutely no effect of IFT on well deliverability is found for Lean Gas B, because $\sigma>\sigma*$ at all $p<p_d$ (Fig. 27).

The potential effect of IFT on well deliverability will be greatest for rich, near-critical fluids producing on decline initially (no plateau). However, for this type of low-permeability well the IFT effect on relative permeabilities will be only one of several major uncertainties (absolute permeability, fracture length, rock relative permeabilities, and oil viscosity). Practically, it will be impossible to separate IFT effects from these other effects, and it also will be difficult to "sell" the optimistic effect of low IFTs to project economics when the IFT/relative permeability phenomena is so poorly understood.

Velocity/IFT Effect. Schulte[20] (and coworkers) at Shell have questioned the validity of using only IFT effect on relative permeabilities for gas condensate systems. They present arguments that indicate an additional improvement in k_{rg} (in addition to low IFT) that might be expected due to high velocities (i.e. pressure drops) experienced near the wellbore. Effectively, they claim that the capillary number (given by the ratio of viscous to capillary forces) should be the correlating parameter instead of IFT (capillarity) alone. Some of their results are to be presented at the 1995 Annual SPE Technical Conference & Exhibition[21].

Subsequently, Henderson et al.[22] provided experimental results of velocity and velocity/IFT effects on relative permeability using Berea sandstone for a five-component

synthetic gas condensate mixture. The two systems used had IFTs of 0.05 and 0.4 mN/m with flowing velocities ranging from 3 to 120 ft/D (10^{-5} m/s to $4 \cdot 10^{-4}$ m/s). The experiments combined a stabilized steady-state flow test followed by interpretation of an unsteady-state flow test.

Fig. 30 shows a plot of the 0.4 mN/m data plotted as k_{rg} vs. k_{rg}/k_{ro} (the 0.05 mN/m data are totally irrelevant to well deliverability). The curve is shifted to higher k_{rg} values at higher velocities, without changing the shape of the curve significantly. Unfortunately, 0.4 mN/m is probably the smallest IFT that can ever be expected in Region 1 (when a well is approaching the minimum BHFP). The net effect of high velocities at more relevant (higher) IFTs has yet to be studied experimentally; we suspect that the effect may "disappear" at higher IFTs (found in most of Region 1), as mentioned by Henderson et al.

Fig. 31 plots k_{rg} (at $k_{rg}/k_{ro}=10$) vs. capillary number N_c ($N_c = \mu_g v_s/\sigma$, where v_s is gas pore velocity) for the six velocity/IFT conditions reported. A clear trend of increasing k_{rg} with N_c is seen. However, the practical range of N_c expected in Region 1 (when a well is approaching the minimum BHFP) is less than about $5 \cdot 10^{-5}$.

The actual profile of N_c in Region 1 needs to be studied in more detail. We suspect note that this profile will be very different in radial and vertically fractured wells. If N_c is small enough (e.g. $<10^{-5}$) in a significant portion of Region 1, then the net IFT/velocity effect on well deliverability is probably small.

Furthermore, near the wellbore where velocity is highest, any positive effect that a high N_c value might have on "Darcy" relative permeability (k_{rg}) may be offset by non-Darcy flow effects. We estimate that Henderson et al.'s highest-velocity data are just on the limit of Darcy flow (based on a Reynold's number of about 0.5 to 1, as defined by Muskat[2,12]).

Conclusions

1. Gas condensate wells producing with BHFP below the dewpoint have up to three flow regions. *Region 1* has a constant flowing composition (GOR) where both gas and oil flow simultaneously. Most of the deliverability loss is caused by reduced gas permeability in Region 1. *Region 2* is where condensate accumulates but has no mobility. *Region 3* is the outer region where reservoir pressure is greater than the dewpoint and only gas flows.

2. Gas well deliverability can be accurately determined using a simple rate equation, Eq. (1) or Eq. (2). The multiphase pseudopressure function is easily calculated from producing GOR (composition) and PVT properties. The effect of reduced gas permeability (condensate blockage) is incorporated in the pseudopressure function. All other well terms (well geometry, damage skin, etc.) are accounted for in the "productivity" constant C. The method is shown to work for radial, vertically fractured, and horizontal wells.

3. The multiphase pseudopressure function is calculated in three parts, based on the three flow regions. Region 1 pseudopressure is calculated using the Evinger-Muskat approach, modified for gas condensate systems. Region 2 uses

the $k_{rg}(S_o)$ relationship, and $S_o(p)$ estimated from the liquid dropout curve from a CVD experiment. Region 3 pseudopressure is the same as for single phase gas.

4. Local grid refinement is not needed for gas condensate wells in full-field models. The proposed pseudopressure method calculates well deliverability accurately in coarse grid models, without any near-well grid refinement. Examples are given for radial, vertically fractured, and horizontal wells.

5. The primary relative permeability relationship affecting condensate blockage (in Region 1), and thus the primary cause of reduced well deliverability, is k_{rg} as a function of k_{rg}/k_{ro}. Saturation does not enter the calculation.

6. Critical oil saturation S_{oc} has no effect on gas condensate well deliverability.

7. Gas-oil interfacial tension has little effect on gas condensate well deliverability (unless a physically questionable model is used for the dependence of relative permeability on IFT).

8. An experimental procedure is recommended for obtaining the key relative permeability data needed to properly model gas condensate well deliverability.

9. Deliverability of horizontal gas condensate wells is strongly affected by the k_v/k_h ratio. Severe deliverability loss is shown even for a normal k_v/k_h ratio of 0.1, compared with the performance of the same horizontal well with $k_v/k_h=1$.

Nomenclature

B_{gd}	=	dry gas FVF, RB/scf or m^3/m^3
B_o	=	oil FVF, RB/STB or m^3/m^3
C	=	gas rate constant
F	=	IFT correlating parameter
G	=	Current surface gas in place in CVD cell, scf or m^3
h	=	reservoir thickness, ft or m
J	=	productivity index, scf/D/psi or $m^3/s/Pa$
k	=	absolute permeability, md (μm^2)
k_r	=	relative permeability (generic)
k_{rg}	=	gas relative permeability
k_{ro}	=	oil relative permeability
k_v/k_h	=	vertical-to-horizontal permeability ratio
L	=	core length, ft or m
M_g	=	gas molecular weight
M_o	=	oil molecular weight
n	=	exponent in IFT correction
N	=	Current STO in place in CVD cell, STB or m^3
N_c	=	Dimensionless viscous-to-capillary number
p	=	pressure, psia or Pa
p^*	=	pressure at outer boundary of Region 1, psia or Pa
p_d	=	dewpoint pressure, psia or Pa
Δp	=	total pressure drop (across core), psi or Pa
Δp_p	=	total pseudopressure, psi/cp or 1/s
p_R	=	average reservoir pressure, psia or Pa
p_{sc}	=	standard condition pressure, psia or Pa
p_{wf}	=	wellbore flowing pressure, psia or Pa
q_g	=	surface gas rate, scf/D or m^3/s
$q_{g,core}$	=	gas flow rate at core conditions, ft^3/D or m^3/s
$q_{o,core}$	=	oil flow rate at core conditions, ft^3/D or m^3/s
q_{inj}	=	pump injection rate, ft^3/D or m^3/s

r_e = external drainage radius, ft or m
r_s = solution OGR, STB/scf or m^3/m^3
r_w = wellbore radius, ft
R = gas constant
R_p = producing GOR, scf/STB or m^3/m^3
R_s = solution GOR, scf/STB or m^3/m^3
s = skin factor
S^* = normalized saturation
S_g = gas saturation
S_o = oil saturation
S_{oc} = critical oil saturation
S_r = residual saturation (generic)
S_w = water saturation
S_{wi} = irreducible water saturation
T = reservoir temperature, °R or K
T_{sc} = standard condition temperature, °R or K
V_d = dewpoint volume, ft^3 or m^3
V_{ro} = CCE oil relative volume, $V_o/(V_g+V_o)$
V_{ro} = CVD oil relative volume, V_o/V_d
V_{rt} = CCE total relative volume, $(V_g+V_o)/V_d$
v_s = pore velocity = $v/[\phi(1-S_{wi})]$, ft/D or m/s

β_s = surface gas mole fraction in wellstream
λ = Corey pore size distribution factor
μ_g = gas viscosity, cp or Pa·s
μ_o = oil viscosity, cp or Pa·s
ρ_g = gas density, lb/ft^3 or kg/m^3
ρ_o = oil density, lb/ft^3 or kg/m^3
σ = gas-oil IFT, dynes/cm or N/m
σ^* = threshold gas-oil IFT, dynes/cm or N/m
ϕ = porosity

References

1. Evinger, H.H. and Muskat, M.: "Calculation of Theoretical Productivity Factor," *Trans.*, AIME (1942) **146**, 126-139.

2. Muskat, M.: *Physical Principles of Oil Production*, McGraw-Hill Book Company, Inc. (1949).

3. Fetkovich, M.J.: "The Isochronal Testing of Oil Wells," paper SPE 4529 presented at the 1973 SPE Annual Technical Conference and Exhibition, Las Vegas, Sept. 30-Oct. 3.

4. Kniazeff, V.J. and Naville, S.A.: "Two-Phase Flow of Volatile Hydrocarbons," *SPEJ* (March 1965) 37-44; *Trans.*, AIME, **234**.

5. Eilerts, C.K., Sumner, E.F., and Potts, N.L.: "Integration of Partial Differential Equation for Transient Radial Flow of Gas-Condensate Fluids in Porous Structures," *SPEJ* (June 1965) 141-152.

6. Eilerts, C.K. and Sumner, E.R.: "Integration of Partial Differential Equations for Multicomponent, Two-Phase Transient Radial Flow," *SPEJ* (June 1967) 125-135.

7. Gondouin, M., Iffly, R., and Husson, J.: "An Attempt to Predict the Time Dependence of Well Deliverability in Gas Condensate Fields," *SPEJ* (June 1967) 112-124; *Trans.*, AIME, **240**.

8. O'Dell, H.G. and Miller, R.N.: "Successfully Cycling a Low Permeability, High-Yield Gas Condensate Reservoir," *JPT* (Jan. 1967) 41-47; *Trans.*, AIME, **240**.

9. Fussell, D.D.: "Single-Well Performance Predictions for Gas Condensate Reservoirs," *JPT* (July 1973) 258-268, 860-870; *Trans.*, AIME, **255**.

10. Jones, J.R. and Raghavan, R.: "Interpretation of Flowing Well Response in Gas Condensate Wells," paper SPE 14204 presented at the 1985 SPE Annual Technical Conference and Exhibition, Las Vegas, Sept. 22-25.

11. Jones, J.R., Vo, D.T., and Raghavan, R.: "Interpretation of Pressure Buildup Responses in Gas Condensate Wells," paper SPE 15535 presented at the 1986 SPE Annual Technical Conference and Exhibition, New Orleans, Oct. 5-8.

12. Golan, M. and Whitson, C.H.: *Well Performance*, 2nd ed., Prentice-Hall (1986).

13. Earlougher, R.C., Jr.: *Advances in Well Test Analysis*, Monograph, SPE, Dallas (1977).

14. Whitson, C.H. and Torp, S.B.: "Evaluating Constant Volume Depletion Data," *JPT* (March 1983) 610-620; *Trans.*, AIME, **275**.

15. Al-Hussainy, R., Ramey, H.J., Jr., and Crawford, P.B.: "The Flow of Real Gases Through Porous Media," *JPT* (May 1966) 624.

16. Fetkovich, M.D., Guerrero, E.T., Fetkovich, M.J., and Thomas, L.K.: "Oil and Gas Relative Permeabilities Determined From Rate-Time Performance Data," paper SPE 15431 presented at the 1986 SPE Annual Technical Conference and Exhibition, New Orleans, Oct. 5-8.

17. Standing, M.B.: "Notes on Relative Permeability Relationshops," *Proc.*, University of Trondheim, NTH, Norway (1975) .

18. Coats, K.H.: "Simulation of Gas Condensate Reservoir Performance," *JPT* (Oct. 1985) 1870-1886.

19. Peaceman, D.W.: "Interpretation of Well Block Pressures in Numerical Reservoir Simulation," *SPEJ* (1978) 183-194; *Trans.*, AIME 253, .

20. Schulte, A.: "Simulation Mechanisms of Well Impairment Due to Condensate Dropout," SPE Forum Series in Europe, Gas Condensate Reservoirs, Seefeld, Austria (1994).

21. Boom, W., *et al.*: "Experimental Evidence for Improved Condensate Mobility at Near Wellbore Flow Conditions," paper SPE 30766, presented at the 1995 SPE Annual Technical Conference & Exhibition, Oct. 22-25, Dallas.

22. Henderson, G.D., Danesh, A., Tehrani, D., and Peden, J.M.: "The Effect of Velocity and Interfacial Tension on the Relative Permeability of Gas Condensate Fluids in the Wellbore Region," Paper Presented at the 8th European IOR Symposium (May 15-17, 1995), Vienna.

23. Chierici, G.L.: "Novel Relation for Drainage and Imbibition Relative Permeabilities," *Society of Petroleum Engineers Journal* (June 1984) 275-276.

Appendix A.
Measuring Gas Condensate Relative Permeabilities

Based on the simulation work presented in this paper, we have established an experimental procedure for measuring the *key relative permeability data needed for well deliverability*. The most important data (and easiest to measure) is $k_{rg} = f(k_{rg}/k_{ro})$. We recommend that this relation always be determined accurately for k_{rg}/k_{ro} values ranging from a maximum of $k_{rg}/k_{ro}=50$, to a minimum calculated by PVT calculations using Eq. (7) (based on the original reservoir mixture, $R_p=1/r_{si}$).

For Region 2 calculations, it may also be useful to know $k_{rg} = f(S_o)$ at low oil saturations defined by the CVD liquid dropout curve. This data is usually only needed for richer gas condensates where maximum liquid dropout is greater than

about 10%. For leaner systems, the reduction in k_{rg} in Region 2 is negligible, and experimental determination of $k_{rg}(S_o)$ at low oil saturations has little value.

Steady-State Flow (Region 1): $k_{rg} = f(k_{rg}/k_{ro})$. In Region 1, flow near the wellbore is a steady-state process where, at any radius, the mixture entering a volume element ΔV is the same mixture leaving the volume. Practically, a core plug can be considered as such a volume element. Our procedure is based on conducting core plug flow tests that are representative of conditions in Region 1 throughout depletion.

At least five or six steady state points should be measured to define the $k_{rg} = f(k_{rg}/k_{ro})$ relation. Flowing conditions of these data are determined using the PVT-derived plot of $k_{rg}/k_{ro}(p)$ from Eq. (7) [using equally spaced $\log(k_{rg}/k_{ro})$ values], evaluated at the minimum BHFP. An example is shown in **Fig. 32** for Lean Gas B.

The first data is measured using original reservoir fluid. This mixture is flowed through the core at a pressure equal to minimum FBHP until steady state conditions are reached. The pressure drop across the core is used to calculate phase mobilities using

$$k_{rg} = q_{g,core} \frac{L}{kA\Delta p} \mu_g$$

$$k_{rg} = q_{o,core} \frac{L}{kA\Delta p} \mu_o \quad \ldots\ldots\ldots\ldots\ldots\ldots\ldots \text{(A-1)}$$

$$q_{g,core} = q_{inj}(1 - V_{ro,core})\frac{V_{rt,core}}{V_{rt,inj}}$$
$$\ldots\ldots\ldots\ldots\ldots \text{(A-2)}$$
$$q_{o,core} = q_{inj} V_{ro,core} \frac{V_{rt,core}}{V_{rt,inj}}$$

where $V_{ro} = V_o/(V_g + V_o)$ and $V_{rt} = (V_g + V_o)/V_d$ are relative volumes from a CCE test of the flowing reservoir mixture. Subscript "core" indicates the quantity is evaluated at the pressure in the core, and "inj" indicates the quantity is evaluated at the pressure of the injection pump; core and pump temperatures are assumed equal in Eqs. (A-2).

The entire system pressure is brought to a pressure significantly above the original dewpoint. Gas is circulated until the original permeability is obtained, thereby ensuring the original reservoir mixture is contained throughout the system.

The entire system pressure is lowered by removing gas from the system. This results in a depleted reservoir gas (similar to that obtained from a CVD process). This gas mixture is flowed through the core at minimum FBHP until steady state conditions are reached.

Another depletion of the system is made, and the resulting reservoir gas is flowed through the core at minimum FBHP until steady state conditions are reached.

This process is continued until a reservoir gas with $k_{rg}/k_{ro} = 50$ is reached in the core (at minimum FBHP). The system "depletion" pressure of this last data is known from calculations made earlier using Eq. (7).

A plot is made of k_{rg} vs. k_{rg}/k_{ro} using a semilog scale. The relation describing these data are the key to accurate description of well deliverability.

Several steady state points can be measured for a given reservoir gas mixture (if sufficient sample is available). For example, injection rate can be varied to study velocity effects, and to minimize end effects. Flow tests at core pressures greater than minimum BHFP can also be made, e.g. to study the potential effect of IFT on relative permeability (i.e. on the k_{rg} vs. k_{rg}/k_{ro} relationship).

Saturation Measurement for Steady State Test. Although saturations do not need to be measured for each steady state test, we do recommend measuring oil saturation for one test, and preferably the final test. This additional data will help convert the $k_{rg} = f(k_{rg}/k_{ro})$ function to a saturation-dependent relation that can be input to a simulator.

After reaching steady state conditions with the final reservoir gas mixture, flow is stopped. The receiving container is brought to minimum BHFP and the condensed oil is removed temporarily from the system. The remaining gas in the receiving container is compressed to a high pressure, and connected with the core. The compressed gas is used to displace the core at elevated pressure into a second receiving container.

After sufficient displacement at high pressure, flow is stopped, the second receiving container is disconnected from the core and brought to minimum FBHP. Oil volume is measured, where this volume is easily shown to equal the average core oil saturation times pore volume.

Equilibrium Gas Flow (Region 2): $k_{rg} = f(S_o)$. For richer gas condensates, the deliverability loss due to condensate accumulation in Region 2 can also be significant. Here we need to quantify k_{rg} as a function of saturation directly. The procedure recommended for measuring $k_{rg}(S_o)$ uses a CVD type process. At each depletion stage, the *entire* system (core and containers) is brought to equilibrium by removing gas from the system.

At each depletion pressure, equilibrium gas is flowed through the core and pressure drop is measured. k_{rg} is calculated from Eq. (A-1), and saturation is taken from the CVD liquid dropout curve, $S_o = V_{roCVD}(1 - S_{wi})$. Measurements are made at decreasing pressures until the maximum liquid dropout occurs, or until oil flow is observed. A sight glass downstream to the core holder is used to detect oil flowing from the core.

Should relative permeabilities be affected by IFT at the higher pressures, this effect is automatically included in the $k_{rg}(S_o)$ measurements.

Fitting Measured Data to Relative Permeability Model. The measured data must be converted into a form that can be used in reservoir simulation, namely k_{rg} and k_{ro} as functions of saturation(s). This conversion process is readily automated by fitting the parameters in a relative permeability model (Corey[17], Chierici,[23] etc.) to the steady-state k_{rg} vs. k_{rg}/k_{ro} data, and the available saturation data from one or more of the steady state tests.

TABLE 1 -- RESERVOIR PROPERTIES USED IN SIMULATIONS	
Water Compressibility, psi^{-1}	$2.67 \cdot 10^{-6}$
Rock Compressibility, psi^{-1}	$5.00 \cdot 10^{-6}$
Reservoir Height h, ft	200
Porosity ϕ, %	30
Absolute (horizontal) Permeability k, md	6
Relative Permeability at S_{wi}	0.8
Irreducible Water Saturation S_{wi}, %	25
Reservoir Area, acres	650
Gas Plateau Rate, MMscf/D	40
Minimum BHFP p_{wfmin}, psia	1500

TABLE 2 -- KEY RESERVOIR FLUID PROPERTIES	Rich Gas A	Lean Gas B
Initial Reservoir Pressure, psia	6500	5500
Initial Reservoir Temperature, ^{o}F	266	315
Dewpoint Pressure, psia	5900	5400
Maximum CVD Liquid Dropout V_{roCVD}, %	24	2
Initial Solution OGR r_{si}, STB/MMscf	175	45
STO API Gravity, ^{o}API	55	45

Separator conditions. Stage 1 p = 375 psia and T = 108°F, Stage 2 p = 14.7 psia and T = 60°F.

TABLE 3 -- NUMERICAL MODEL GRID DATA.		
Grid Description		**Grid Dimension, ft**
Radial Well Grid		
Radial coordinates. Total radius r_e = 3000 ft.		0.53 0.89 1.39 2.15 3.35 5.20 8.07 12.53 19.46 30.23 36.94 72.9
Skin s = 0 in Eq. (3), used in Eqs. (1)-(2).		113.2 175.01 273.01 423.97 658.41 1022.49 1587.88 2465.9
Vertically Fractured Well Grid		
Cartesian coordinates. One quarter of the well	Δx	2*15 7*10 2*50 3*100 100 100 15*137.2
simulated. Equal model width and length of		
2658.5 ft. Fracture grid k = 10,000 md.	Δy	3 0.83 1.53 2.81 5.15 9.44 17.31 58.24 106.82 195.92 359.34
Skin s = -4 in Eq. (3), used in Eqs. (1)-(2).		659.06 1207.8
Horizontal Well Grid		
Cartesian coordinates. One eighth of the well	Δx	100 2*50 8*10 2*100 2*200 300 400 500 458
simulated (1/2 reservoir height and 1/4 area).		
Equal model width and length of 2658.5;	Δy	3 0.83 1.53 2.81 5.15 9.44 17.31 58.24 106.82 195.92 359.34
model height of 100 ft.		659.06 1207.8
Skin s = -4 in Eq. (3), used in Eqs. (1)-(2).	Δz	3 0.83 1.53 2.81 5.15 9.44 17.31 31.75 28.18
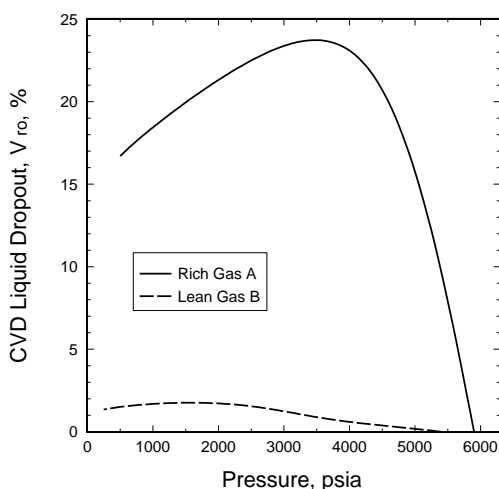
Fig. 1--CVD liquid dropout curves for reservoir fluids Rich Gas A and Lean Gas B.
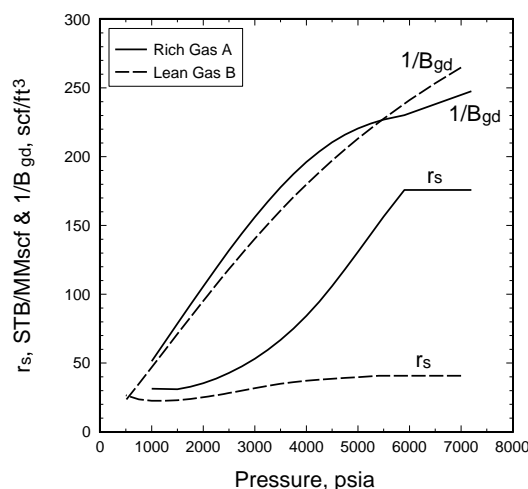
Fig. 2--Black-oil PVT data for Rich Gas A and Lean Gas B. Gas phase properties r_s and B_{gd}.
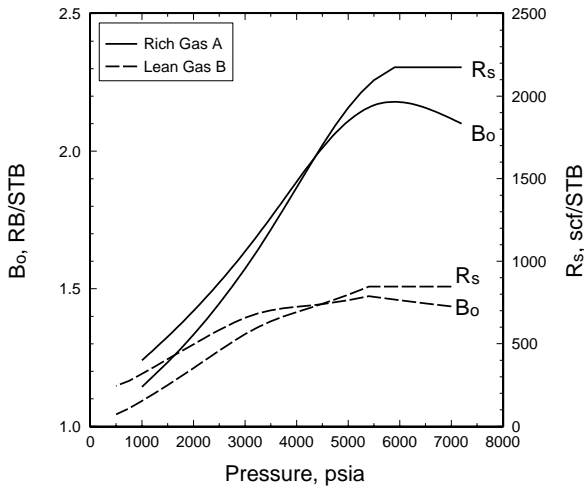
Fig. 3--Black-oil PVT data for Rich Gas A and Lean Gas B. Oil phase properties R_s and B_o.
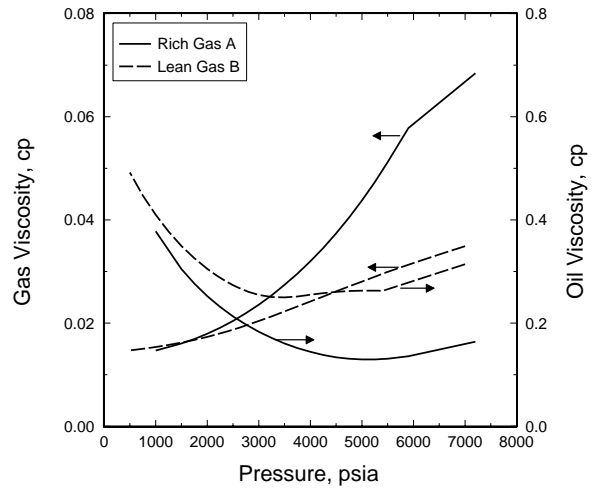
Fig. 4--Black-oil PVT data for Rich Gas A and Lean Gas B. Gas and oil phase viscosities.
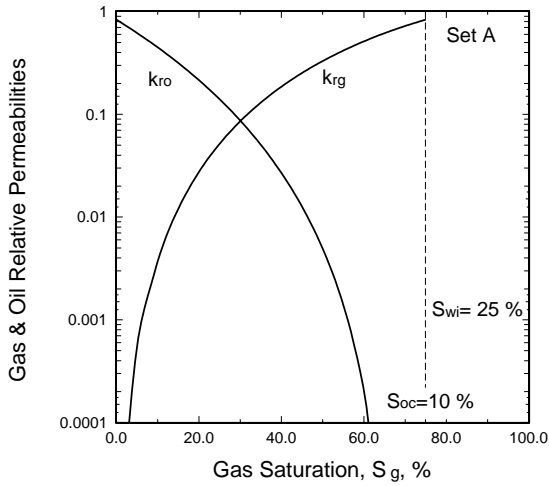
Fig. 5--Set A gas and oil relative permeability curves used in simulations.
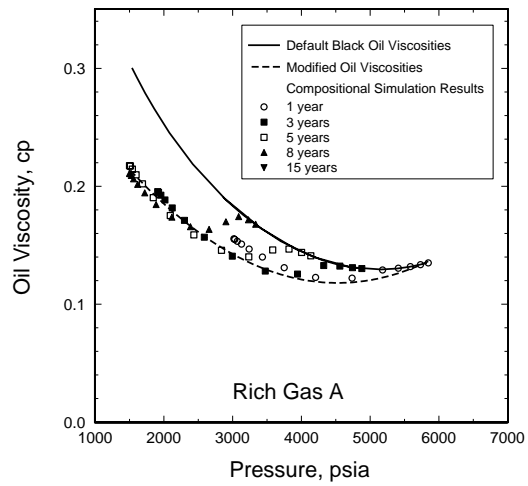
Fig. 6--Changing oil viscosities as a function of pressure for black-oil and compositional PVT models.
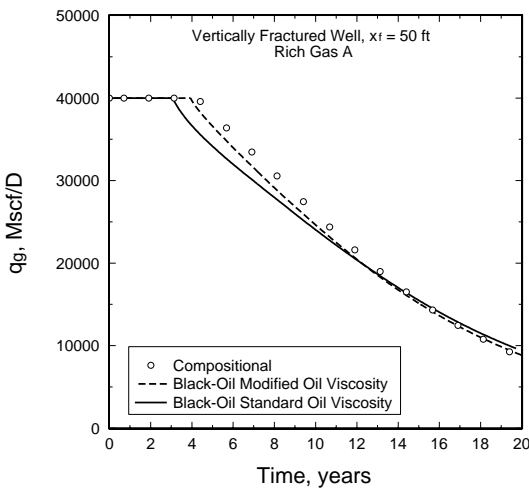
Fig. 7--Effect of oil viscosity on well deliverability for black-oil and compositional simulations of a vertically fractured well with Rich Gas A.
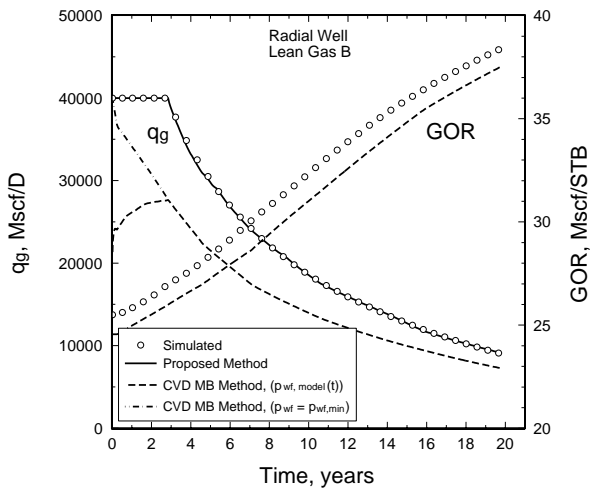
Fig. 8--Well performance for a radial well with Lean Gas B. Comparison of fine-grid simulation with proposed pseudopressure method (and with approximate CVD MB method).
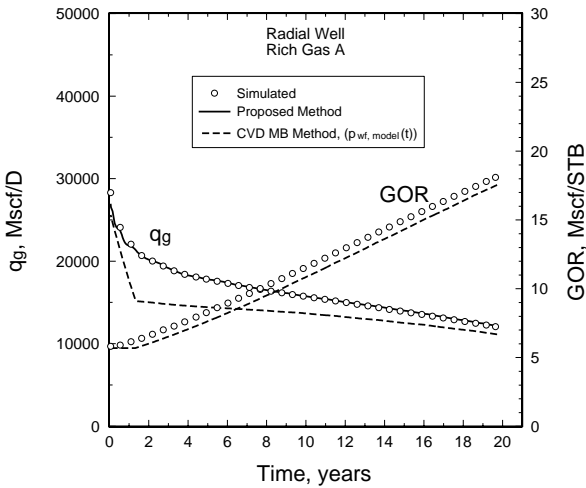
Fig. 9--Well performance for a radial well with Rich Gas A. Comparison of fine-grid simulation with proposed pseudopressure method (and with approximate CVD MB method).
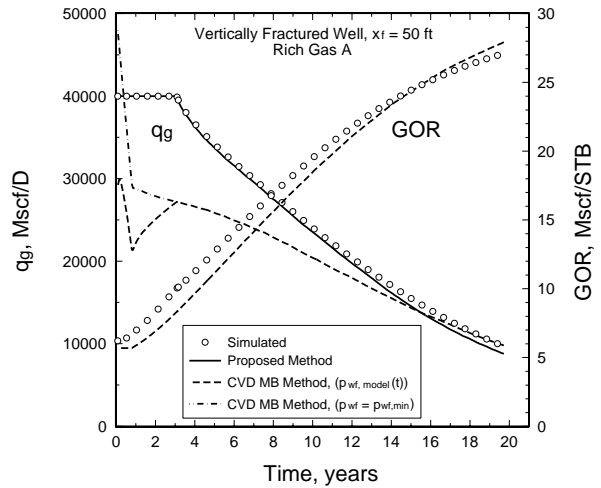
Fig. 10--Well performance for a vertically fractured well with Rich Gas A. Comparison of fine-grid simulation with proposed pseudopressure method (and with approximate CVD MB method).
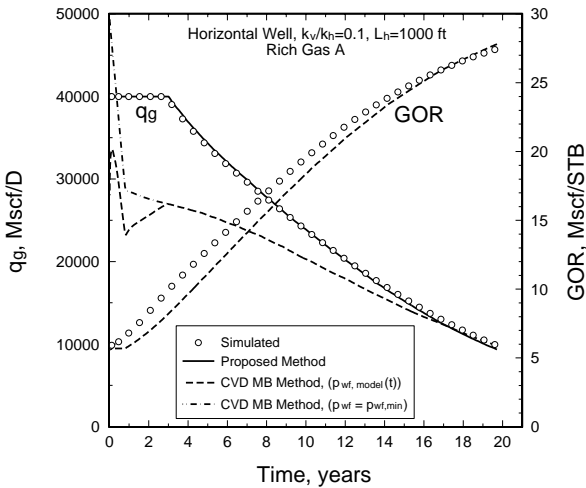
Fig. 11--Well performance for a horizontal well (k_v/k_h=0.1) with Rich Gas A. Comparison of fine-grid simulation with proposed pseudopressure method (and with approximate CVD MB method).
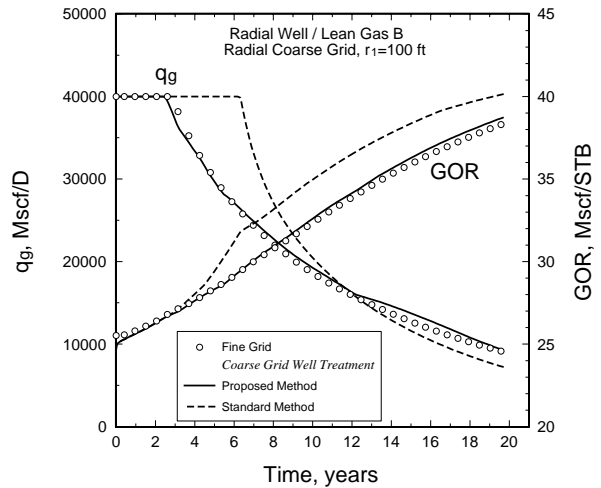
Fig. 12--Well performance for a radial well with Lean Gas B. Comparison of fine-grid simulation with radial coarse-grid simulation using proposed pseudopressure method for calculating well BHFP.
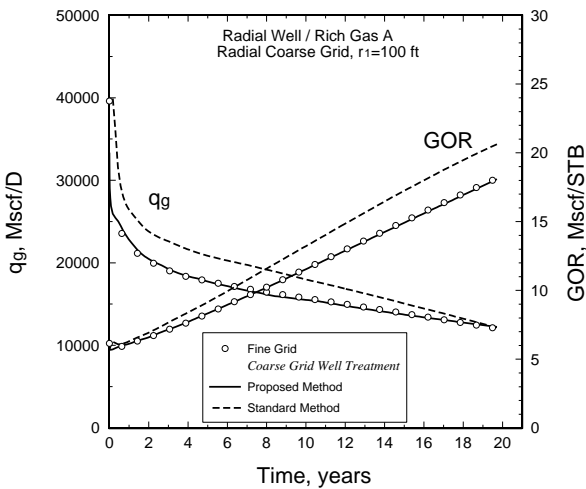
Fig. 13--Well performance for a radial well with Rich Gas A. Comparison of fine-grid simulation with radial coarse-grid simulation using proposed pseudopressure method for calculating well BHFP.
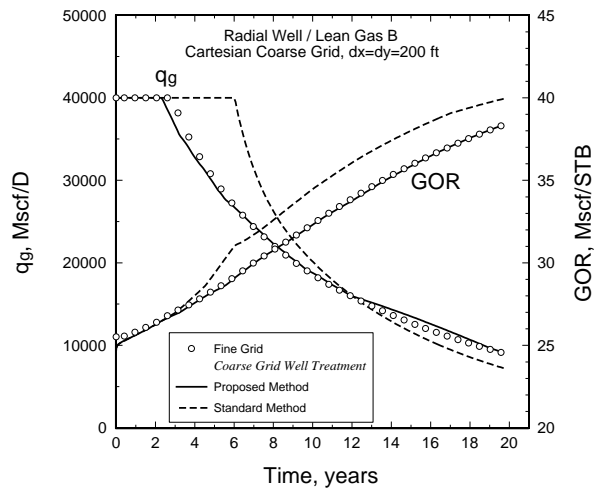
Fig. 14--Well performance for a radial well with Lean Gas B. Comparison of fine-grid simulation with cartesian coarse-grid simulation using proposed pseudopressure method for calculating well BHFP.
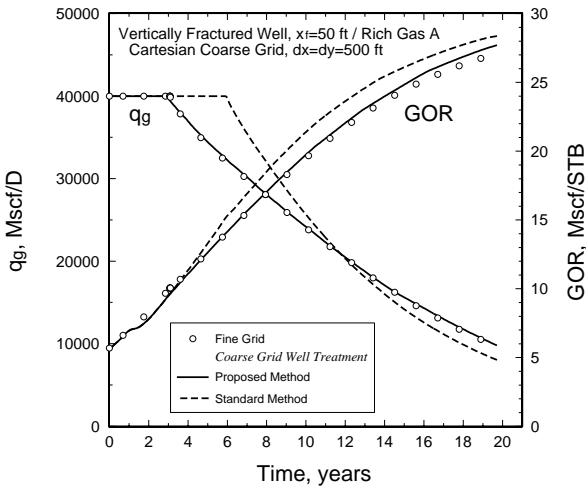
Fig. 15--Well performance for a vertically fractured well with Rich Gas A. Comparison of fine-grid simulation with cartesian coarse-grid simulation using proposed pseudopressure method for calculating well BHFP.
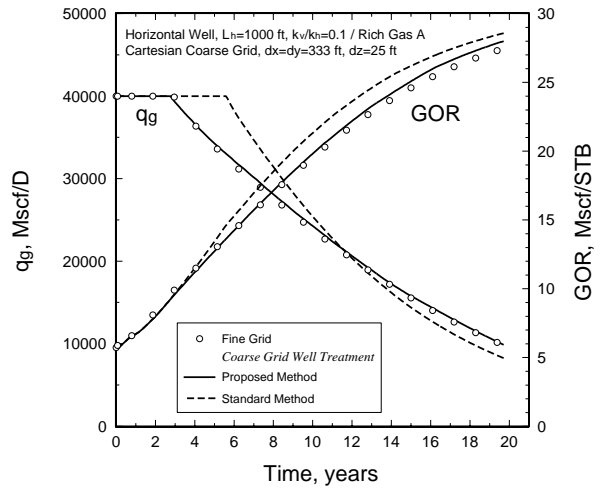
Fig. 16--Well performance for a horizontal well with Rich Gas A. Comparison of fine-grid simulation with coarse-grid simulation using proposed pseudopressure method for calculating well BHFP.
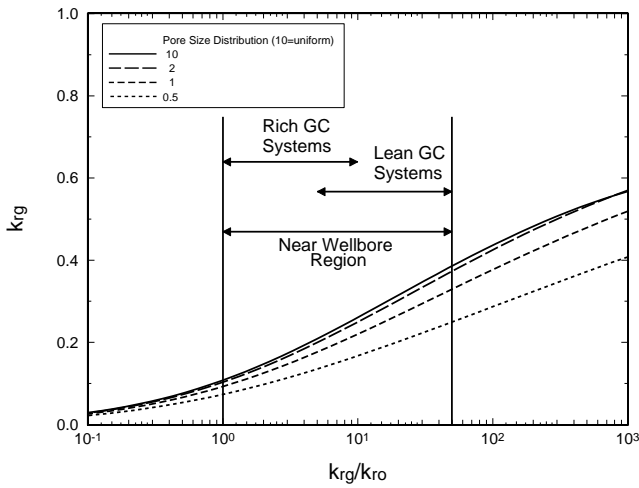
Fig. 17--Generalized k_{rg} vs. k_{rg}/k_{ro} plot based on the Corey relative permeability model. Important range of k_{rg}/k_{ro} in near-wellbore Region 1 is defined.
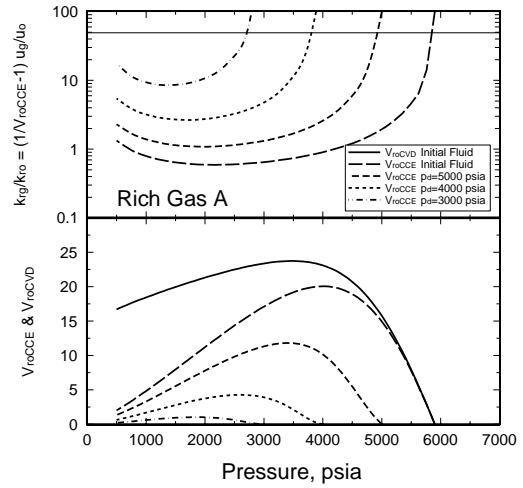
Fig. 18--Diagnostic plots for Rich Gas A showing the variation of k_{rg}/k_{ro} (in Region 1) and CCE oil relative volume as a function of pressure during depletion.
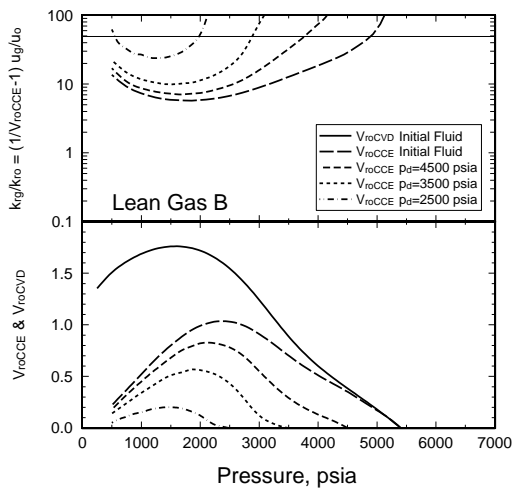
Fig. 19--Diagnostic plots for Lean Gas B showing the variation of k_{rg}/k_{ro} (in Region 1) and CCE oil relative volume as a function of pressure during depletion.
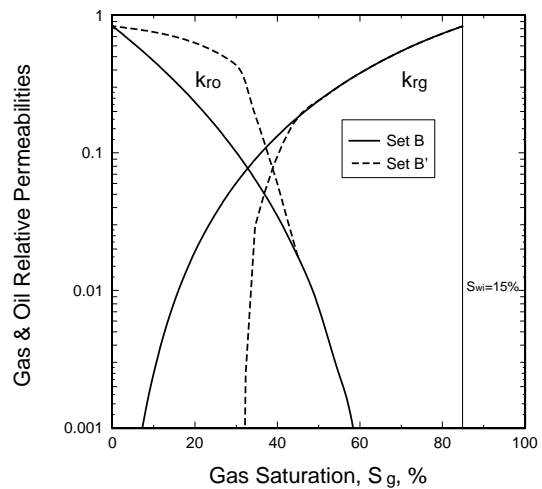
Fig. 20--Two sets of gas/oil relative permeability curves that have identical $k_{rg} = f(k_{rg}/k_{ro})$ relationships.
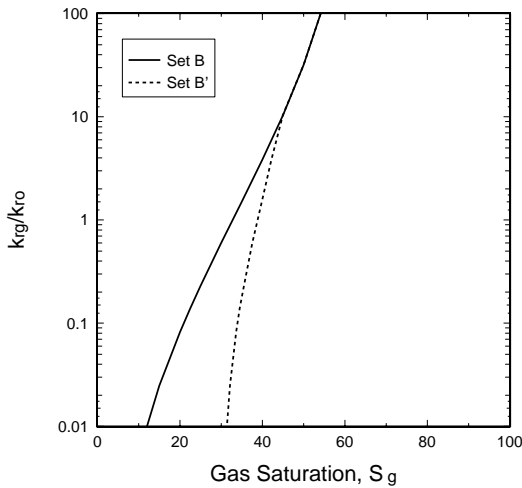
Fig. 21--k_{rg}/k_{ro} vs. S_g for two sets of gas/oil relative permeability curves that have identical $k_{rg} = f(k_{rg}/k_{ro})$ relationships.
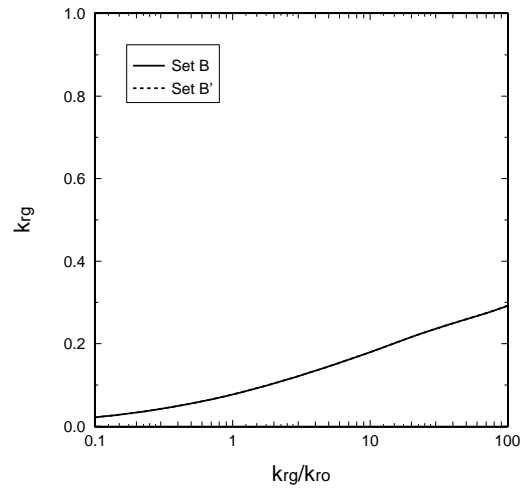
Fig. 22-- Identical $k_{rg} = f(k_{rg}/k_{ro})$ relationship for two completely different sets of $k_{rg}(S_g)$ and $k_{ro}(S_g)$ curves.
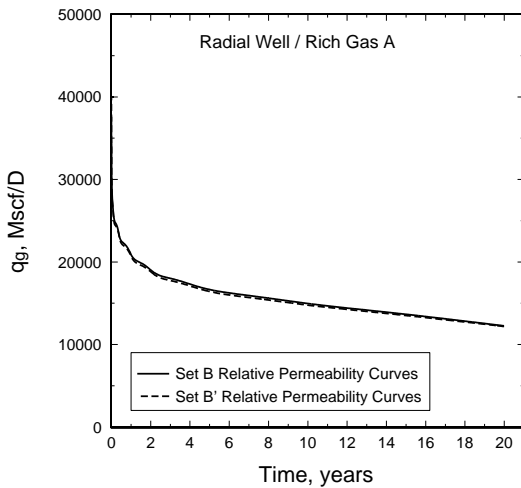
Fig. 23--Rate-time performance of a radial well with Rich Gas A, based on fine-grid simulations using two dramatically different sets of gas/oil relative permeabilities (see Fig. 20).
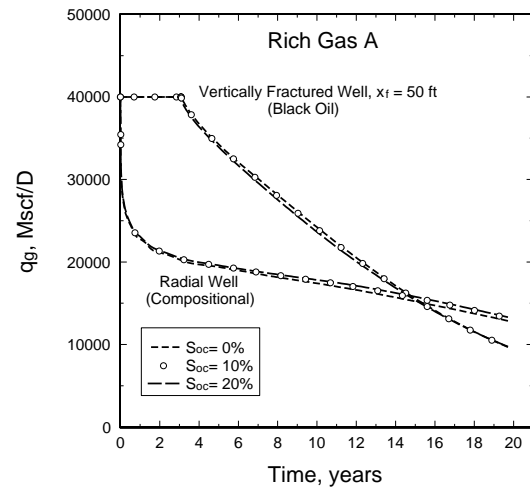

Fig. 24--Rate-time performance of radial and vertically-fractured wells with Rich Gas A, showing the insensitivity of well performance to critical oil saturation S_{oc} (see Fig. 25).
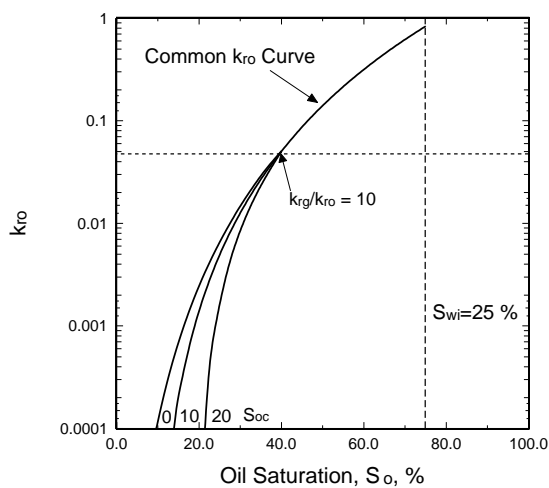
Fig. 25--Variation of k_{ro} curve as a function of oil saturation used in simulations. $k_{ro}(S_o)$ is *unaltered* for $k_{rg}/k_{ro}<10$ ($k_{ro}>0.05$).
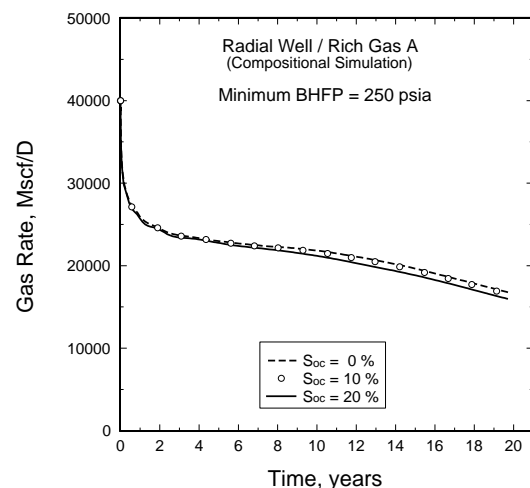
Fig. 26--Rate-time performance of radial well with Rich Gas A, showing the insensitivity of well performance to critical oil saturation S_{oc} (see Fig. 25).
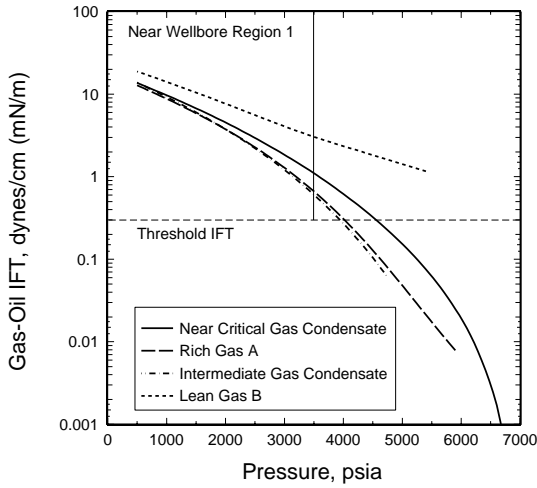
Fig. 27--General pressure dependence of gas-oil IFT for different gas condensate systems.
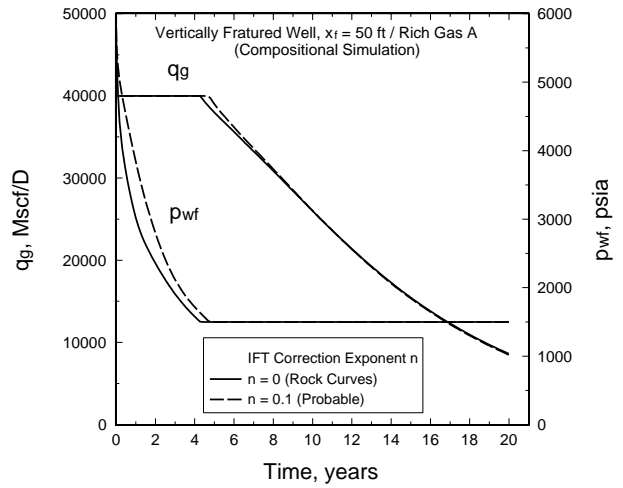

Fig. 28--Well performance of a vertically fractured well with Rich Gas A, based on fine-grid compositional simulations with and without IFT corrections to relative permeability.
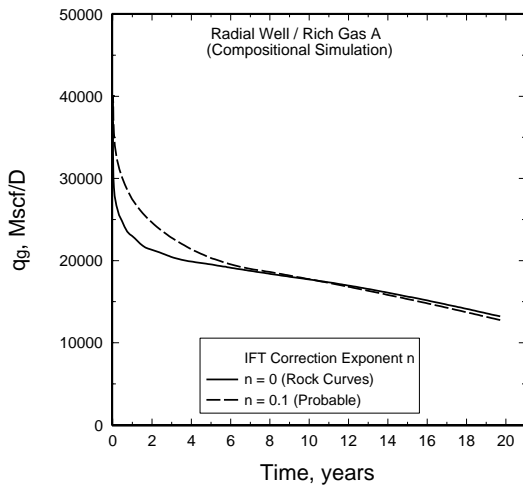

Fig. 29--Well performance of a radial well with Rich Gas A, based on fine-grid compositional simulations with and without IFT corrections to relative permeability.
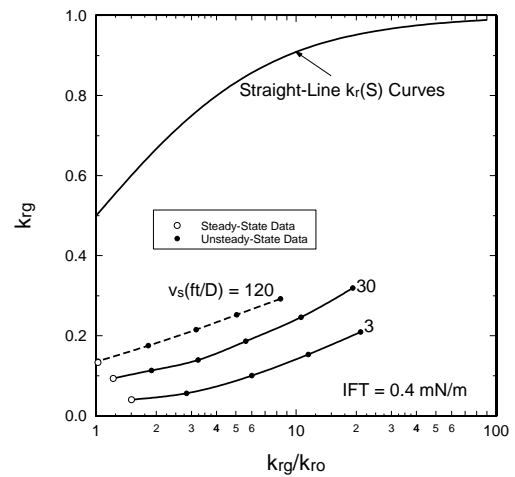

Fig. 30--Velocity effects on $k_{rg} = f(k_{rg}/k_{ro})$ relationship for a Berea sandstone and synthetic gas condensate mixture at IFT of 0.4 mN/m. Data taken from Henderson et al.
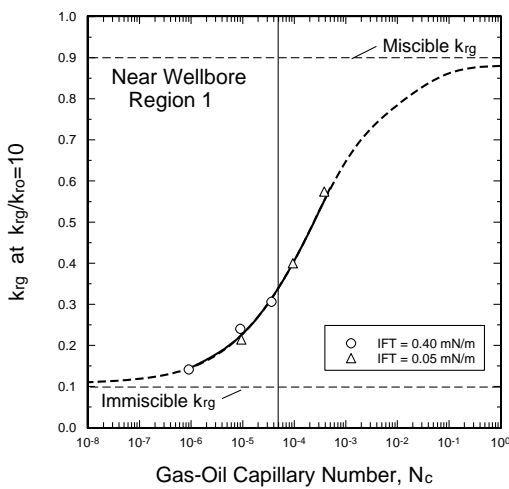

Fig. 31--Combined velocity/IFT effect on k_{rg} as a function of gas/oil capillary number for data presented by Henderson et al.
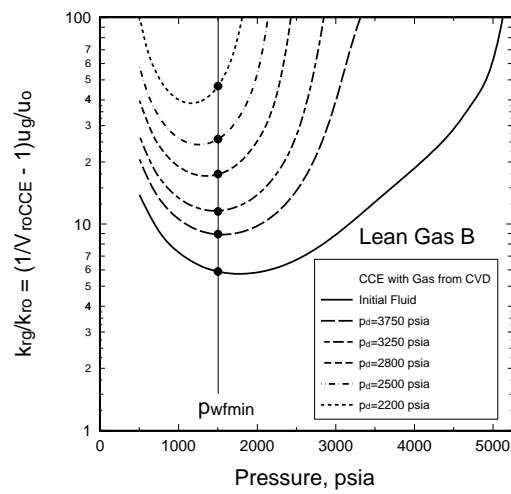

Fig. 32--Design plot for Lean Gas B showing the range of k_{rg}/k_{ro} values that should be measured experimentally for accurate modeling of well deliverability.